Microstructure and dielectric relaxor properties for $Ba_{0.5}Sr_{0.5}TiO_3/La_{0.67}Sr_{0.33}MnO_3$ heterostructure

J. Miao,[a] H. Y. Tian, X. Y. Zhou, K. H. Pang, and Y. Wang
Department of Applied Physics and Materials Research Center, The Hong Kong Polytechnic University, Hong Kong SAR, People's Republic of China

(Received 28 November 2006; accepted 25 February 2007; published online 16 April 2007)

Ferroelectric and magnetoresistance heterostructure $(Ba,Sr)TiO_3/(La,Sr)MnO_3$ (BST/LSMO) heterostructure is deposited epitaxially on $SrTiO_3$ (001) substrate by pulse laser deposition. The phase structures of the BST/LSMO heterostructure are characterized by x-ray diffraction. Cross-sectional transmission electron microscope shows a substantial interdiffusision between BST and LSMO layers. The dielectric properties and conductivity of BST/LSMO heterostructure is measured as a function of temperature, frequency, and electric field. The dielectric constant dependence on electric field, ε vs E, exhibits a strong nonlinear behavior in the temperature from 20 to 300 K, while $\varepsilon_{(E=0)}$ vs T relation shows a dielectric relaxor characteristic. Furthermore, the dielectric constant ($E=0$ kV/cm) and the dielectric tunability ($E=200$ kV/cm) are found to be similar temperature dependencies. Last, in the temperature regime where a semiconduction-type conduction became dominate, the activation thermal energy of BST/LSMO heterostructure is estimated to be 0.67 and 0.73 eV at 1 kHz and 1 MHz, respectively. © *2007 American Institute of Physics*. [DOI: 10.1063/1.2721393]

I. INTRODUCTION

Recently, ferroelectric barium strontium titanate $(Ba,Sr)TiO_3$ has been investigated extensively for application in dynamic random access memory (DRAM) and tunable microwave devices, due to its high relative dielectric constant, low dielectric loss, and strong tunability under an external electric field.[1,2] On the other hand, the bottom electrode material has an important influence on the dielectric and ferroelectric properties of $(Ba,Sr)TiO_3$ film. In order to obtain high performance of $(Ba,Sr)TiO_3$ film, the bottom electrode layer should have high metallic conductivity, sufficient resistance to oxidation, a smooth surface, and good adhesion to the film. In the past years, conductive oxide materials, such as IrO_2, $SrRuO_3$ (SRO), $LaNiO_3$ (LNO), $La_{0.5}Sr_{0.5}CoO_3$ (LSCO), and $YBa_2Cu_3O_7$ (YBCO)[3–7] have been found to be attractive alternatives, due to their lattice and chemistry matching, high diffusion barrier for oxygen, and phase stability during deposition at high temperature.

Meanwhile, colossal magnetoresistance materials $(La,Sr)MnO_3$ with hole doping attracted interest as candidate materials for the bottom electron layer. As a matter of fact, LSMO has some very attractive features. First $(La_{1-x}Sr_x)MnO_3$ ($x=0.67$) is a perovskite oxide with a lattice parameter of 3.873 Å and has a good match with $(Ba,Sr)TiO_3$ films. When fully oxygenated, the $La_{0.67}Sr_{0.33}MnO_3$ film shows good ferromagnetic metallic phase with Curie temperature about 360 K and relatively low resistivity (~ 1 mΩ Cm). Second, the electrical resistivity of epitaxial $La_{0.67}Sr_{0.33}MnO_3$ film can be controlled by varying the deposition oxygen pressure and remains stable against further thermal treatments in various oxygen pressures.[8] Such properties make $La_{0.67}Sr_{0.33}MnO_3$ film uniquely fit to be used as the bottom electrode layer, in comparison with other perovskite conductive oxides. Moreover, the use of $La_{0.67}Sr_{0.33}MnO_3$ as electrode materials for ferroelectric film may lead to a different class of multifunctional heterostructure, which possesses both ferroelectric and magnetic properties.[9] However, there are few investigations of the microstructure and dielectric properties of $(Ba,Sr)TiO_3/(La,Sr)MnO_3$ heterostructure in the low-temperature region.

In this article, the $(Ba,Sr)TiO_3/(La,Sr)MnO_3$ (abbreviated as BST/LSMO) heterostructure was fabricated on $SrTiO_3$ (001) substrate by pulse laser deposition (PLD) method. The interfacial structure of the BST/LSMO heterostructure was characterized by scanning electron microscopy (SEM) and transmission electron microscopy (TEM). Moreover, the dielectric response of BST/LSMO heterostructure as a function of electric field has been investigated in the temperature range from 20 to 300 K. Last, the conductivity behaviors of the BST/LSMO heterostructure were discussed under the thermal activated process at different temperature and frequency.

II. EXPERIMENTAL DETAILS

Stoichiometric-sintered $Ba_{0.5}Sr_{0.5}TiO_3$ (BST) and $La_{0.67}Sr_{0.33}MnO_3$ (LSMO) ceramic targets were prepared by the conventional solid-state reaction method. The BST and LSMO films were deposited *in situ* on (001) $SrTiO_3$ (STO) substrate by PLD method. A XeCl excimer pulsed laser beam (Lambda Physik Compex205, $\lambda=308$ nm, $\tau=28$ ns) was introduced into the chamber. Initially, a LSMO layer was grown at 820 °C in oxygen pressure of 50 Pa. A laser energy density of 1.5 J/cm^2 and a repetition rate of 3 Hz were used. After deposition, the LSMO layer was annealed at 880 °C for

[a]Electronic mail: j.miao@fz-juelich.de

 © 2007 American Institute of Physics

Downloaded 01 Apr 2011 to 158.132.161.9. Redistribution subject to AIP license or copyright; see http://jap.aip.org/about/rights_and_permissions

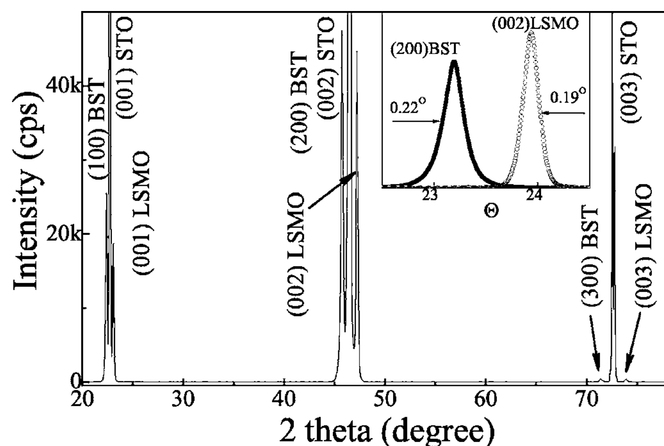

FIG. 1. X-ray diffraction θ-2θ scan of BST/LSMO heterostructure on STO substrate. The insert shows ω-rocking scans of the (002) BST and (002) LSMO peaks for the BST/LSMO heterostructure.

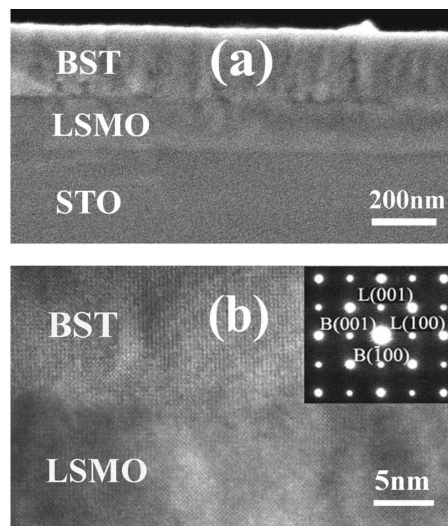

FIG. 2. (a) Cross-sectional FE-SEM image obtained from BST/LSMO//STO heterostructure. (b) High-resolution TEM bright-field image obtained at the interface of BST/LSMO heterostructure. The inset shows the corresponding SAED pattern at the BST/LSMO interface.

30 min in oxygen with pressure near 1 atmosphere. The BST layer was then deposited *in situ* on top of the LSMO layer at 800 °C in oxygen with a pressure of 30 Pa, for which a laser energy density of 2 J/cm^2 and a repetition rate of 5 Hz were adopted. After deposition, the as-deposited heterostructure was annealed in oxygen pressure near 1 atmosphere at 600 °C for 30 min; then it was cooled down to room temperature slowly. The thickness of LSMO and BST layers was measured by a cross-sectional scanning electron microscopy.

The phase structures of the BST/LSMO heterostructure were characterized by x-ray diffraction (XRD, MacScience, M18XHF, Cu $K\alpha$ radiation) using θ-2θ scan, ω-rocking curve, and φ scan. Field-emission scanning electron microscopy (FESEM, Leico, Stereo scan440) and transmission electron microscopy (TEM, JEOL2010) were used to examine the interfacial microstructure. For electrical properties measurement, 200 nm Pt top electrodes were deposited on the top of BST/LSMO heterostructure by magnetron sputtering through a shadow metal mask. The area of the Pt electrode was restricted within 8×10^{-3} cm^2 and the distance between them was about 3 mm. The dc electric field dependence of dielectric properties of BST/LSMO heterostructure was measured using a HP4284a precision LCR meter in the temperature range from 20 to 300 K. During the dielectric measurements, the bias voltage was swept from negative to positive and then back to negative with a rate of 0.4 V/s with elapsed time of 30 s. The temperature dependence of ac conductivity of BST/LSMO heterostructure was measured under 1×10^4 V/cm in the frequency range from 1 kHz to 1 MHz.

III. RESULTS AND DISCUSSION

Figure 1 shows a typical θ-2θ XRD scan of BST/LSMO heterostructure deposited on a (001) $SrTiO_3$ single crystal. Only the (00*l*) peaks of BST and LSMO films were observed, indicating that both BST and LSMO layers grew epitaxially with the *c*-axes normal to $SrTiO_3$ substrate surface. In order to confirm the epitaxial growth and crystallization of the BST/LSMO heterostructure, ω-rocking curves and φ-scan measurements were also carried out. The inset of Fig. 1 shows the ω-rocking curves of the peaks of (200) BST and (002) LSMO. The full-width at half-maximum (FWHM) of the (200) BST and (002) LSMO peaks were 0.22° and 0.19°, respectively, indicating that the BST/LSMO heterostructure grown under these conditions have a good crystallinity. Moreover, the epitaxial nature of both the BST and LSMO layers is demonstrated by the in-plane orientation with respect to the major axes of the substrate. From the XRD φ-scan (not shown here), the fourfold symmetry of the φ-scan of the (101) BST, (101) LSMO, and (101) STO peaks exhibits the following cube-on-cube epitaxial relationship:

$$(001)\mathrm{BST}//(001)\mathrm{LSMO}//(001)\mathrm{STO},$$

$$[100],[010]\mathrm{BST}//[100],[010]\mathrm{LSMO}//[100],[010]\mathrm{STO}, \quad (1)$$

where the crystallographic planes of BST and LSMO layers are presented in the pseudocubic structure.[10]

Figure 2(a) shows the cross-sectional FESEM image of BST/LSMO heterostructure deposited on (001) STO substrate. From the SEM result, the film thicknesses of BST and LSMO layers are estimated to be 240 and 150 nm, respectively. Moreover, the typical columnar microstructure in BST film was shown as the dark-bands contrast, which has been also observed in ferroelectric films grown on $SrTiO_3$ and MgO single crystal.[11,12] As shown in the figure, the presence of an interfacial layer between BST and LSMO layers is not evident. However, its existence cannot be excluded since the presence of such a thin interfacial layer might be faded, due to the charging effect of the dielectric film under electron radiation.[13] To investigate the interfacial state and epitaxial quality, a cross-sectional TEM was performed at the interface between BST and LSMO layers.

Figure 2(b) shows the lattice fringe image of BST/LSMO interface using high-resolution TEM (HRTEM). From the figure, the epitaxial growth and high degree of crystallinity of both BST and LSMO layers could be con-

Downloaded 01 Apr 2011 to 158.132.161.9. Redistribution subject to AIP license or copyright; see http://jap.aip.org/about/rights_and_permissions

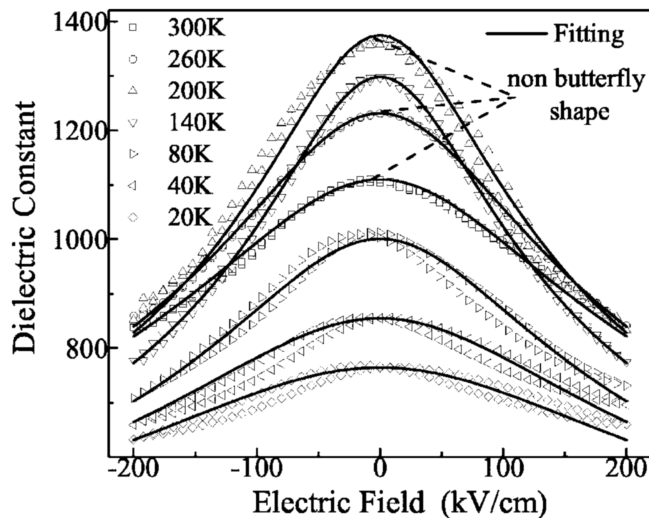

FIG. 3. dc electric field dependence of dielectric constant for Pt/BST/LSMO capacitor in the temperature range from 20 to 300 K (at 100 kHz). The experimental data were fitted following the Johnson's formula as the solid lines (see the text).

firmed for a certainty. However, an interdiffusive regime between BST and LSMO layers is observed on the order of 3 nm, indicating elemental diffusion occurred at the interface of the heterostructure. The existence of interdiffusive layer has been unambiguously supported by the Auger electron spectroscopy (AES) depth analysis.[14] As for the origin, the interfacial layer between BST and LSMO layers may be formed during the fabrication of heterostructure at temperature of 800 °C or even higher. From LSMO layer, La and Mn ions diffused into the ferroelectric layer, whereas Ba and Ti diffused from the ferroelectric layer into LSMO layer. Similar phenomenon has been reported previously in the $(Ba,Sr)TiO_3/LaNiO_3$ (Ref. 15) and $PbTiO_3/(La,Sr)MnO_3$ structures.[16] As a result, the formation of such an interdiffusive layer may have great influence on the electrical properties of BST/LSMO heterostructure. Furthermore, to analyze the crystallization and epitaxial behavior, a pattern of selected area electron diffraction (SAED) was taken from the area covering the interface of BST and LSMO films. As shown in the inset of Fig. 2(b), the sharp electron diffraction spots of the heterostructure without satellite peaks indicated that both BST and LSMO layers have good crystallinity. Moreover, from the figure, the orientation relationships of BST/LSMO heterostructure can be confirmed as the following: [001],[100]BST//[100],[001]LSMO. This conclusion is consistent with the results of the φ-scan of XRD.

Figure 3 shows the dc electric field dependence of dielectric constant for BST/LSMO heterostructure in the temperature range from 20 to 300 K. This measurement is carried out at the frequency of 100 kHz with a small oscillation voltage of 200 mV. As seen from the figure, the value of T_C of BST/LSMO heterostructure is around 200 K at 100 kHz. Moreover, with temperature decreasing, the dielectric permittivity of the films grows until 200 K, and then it decreases with decreasing of temperature. This phenomenon is attributed to the formation in BST film of the large size domains in the low temperature. Furthermore, it is found that the ε vs E characteristics exhibit a butterfly-shaped behavior with temperature below 200 K, and show a relatively weak hysteresis behavior above 200 K. This phenomenon is explained as follows: as temperature decreases, the ferroelectric domain wall movement in BST film becomes more difficult and the amount of switchable polarizations increase. Miller *et al.*[17] pointed out that the peak (maximum of permittivity) in the ε vs E characteristics of ferroelectric capacitors corresponds to a reversal of the polarizations, and the amplitude corresponds to the amount of switchable polarizations. Therefore, with decreasing temperature below T_C, the amount of switchable polarization in BST films was increased, which led to the higher magnitude of peaks. As a consequence, with decreasing temperature, the pronounced butterfly shape of ε vs E characteristics for BST/LSMO heterostructure became more obvious, indicating the ferroelectricity of BST film is enhanced in the lower temperature regime. However, above the transition temperature, the BST film is in the paraelectric state, while ε vs E characteristics exhibit a faint hysteresis behavior.

The explicit relationship between applied electric field and dielectric constant can be qualitatively interpreted by the phenomenological theory proposed by Johnson.[18] In the case of $\varepsilon_{r(T,0)} \gg 1$, the electric field dependence of dielectric constant can be expressed as follows:

$$\varepsilon_{r(T,E)} = \frac{\varepsilon_{r(T,0)}}{[1+(\varepsilon_0\varepsilon_{r(T,0)})^3\alpha_{(T)}E^2]^{1/3}}, \quad (2)$$

where $\varepsilon_{r(T,0)}$ and $\varepsilon_{r(T,E)}$ are the dielectric constants at zero electric field and applied electric field E, respectively, and $\alpha_{(T)}$ is the temperature-dependent constant, which provides information on the degree of enharmonic contributions of the polarization to the free energy.[19] Equation (2) predicts that the broadened extent of ε vs E characteristics depended on the temperature dependence of $\varepsilon_{r(T,0)}$, which decreases above and below T_C according to the Curie-Weiss law. Therefore, the experimental data of ε vs E characteristics at zero field are fitted using Eq. (2) as the solid lines. As shown in Fig. 3, in the paraelectric state above T_C, the ε vs E characteristics can be fitted exactly over the whole electric field range. The deviations of the data from the fitting line are less than 2%. However, there are two branches of the experimental curve (butterfly-shape hysteresis) in the ferroelectric state, which originated from the dipolar movement in the BST/LSMO heterostructure. Moreover, it can be seen that the observed hysteresis in BST/LSMO heterostructure is not so large in the low temperature. Thus, we fit Eq. (2) with the value of $[\varepsilon_{r(+)}+\varepsilon_{r(-)}]/2$, where $\varepsilon_{r(+)}$ is the branch sweeping from positive to negative field and $\varepsilon_{r(-)}$ is the reversed one. As a result, the agreement between the ε vs E curves and the fitting lines of BST/LSMO heterostructure is quite good. Therefore, the predicted curves from Eq. (2) and the measurements are in good agreement, indicating the self-consistency of that model. Further investigation on the temperature dependence of dielectric properties of BST/LSMO heterostructure will be discussed later.

Figure 4 shows the temperature dependence of the dielectric constant deduced from $\varepsilon_{(E=0)}$ vs T characteristics at

Downloaded 01 Apr 2011 to 158.132.161.9. Redistribution subject to AIP license or copyright; see http://jap.aip.org/about/rights_and_permissions

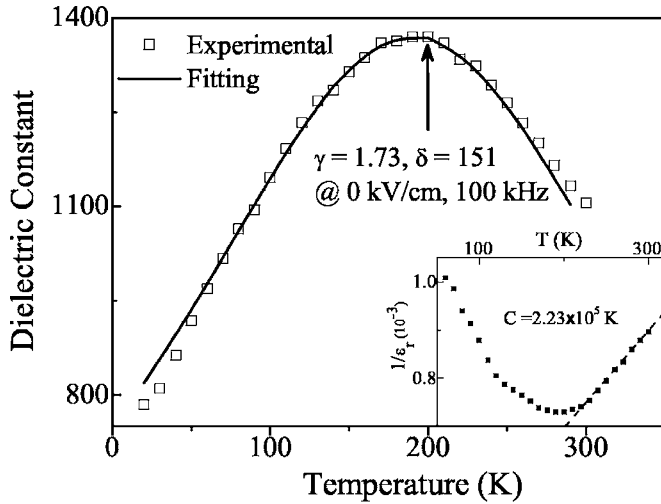

FIG. 4. Temperature dependence of dielectric constant of Pt/BST/LSMO capacitor at 100 kHz and zero field deduced from Fig. 3. The fitting curve shows a dielectric diffusion behavior of the heterostructure. The Curie-Weiss plot of the BST/LSMO heterostructure is shown in the inset.

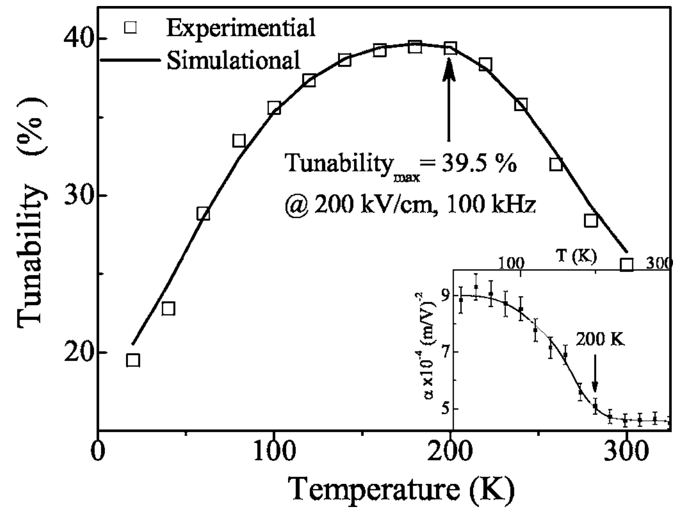

FIG. 5. Temperature dependence of dielectric tunability of Pt/BST/LSMO capacitor at 100 kHz and 200 kV/cm deduced from Fig. 3. The fitting curve was simulated by the Johnson's theory. The inset shows the enharmonic contribution of polarization of the Pt/BST/LSMO capacitor as a function of temperature.

100 kHz. It can be seen that the maximum dielectric constant [$\varepsilon_{\max(E-0)}=1374$] of the BST/LSMO heterostructure was reached in the vicinity of 200 K. Meanwhile, a diffused dielectric characteristic can be observed from the temperature dependence of dielectric constant of the BST/LSMO heterostructure. As is well known, the diffuseness of the dielectric characteristic can be quantified by the relation[20]

$$\frac{1}{\varepsilon_r}=\frac{1}{\varepsilon_{\max}}+\frac{(T-T_{\max})^{\gamma}}{2\varepsilon_{\max}\delta^2}, \tag{3}$$

where $T_{\max}$ is the temperature corresponding to $\varepsilon_{\max}$; δ is a broadening parameter; γ is a constant which character the degree of relaxation: for $\gamma=1$, the material follows an ideal Curie-Weiss law which shows the validity in case of the normal ferroelectrics, whereas $\gamma=2$ indicates a typical ferroelectric relaxor response. We fitted our data with Eq. (3) as indicated by the solid line in Fig. 4, from which the value of γ is estimated as 1.73. However, the fitting to Eq. (3) cannot use a criterion as a relaxor or not, because the hallmark of the relaxor is a broad relaxation spectrum which appears as frequency dependence of the $T_{\max}$. Further investigation will be done on the low-T frequency dispersion of relaxation spectrum of BST/LSMO heterostructure. The large value of γ obtained here may be attributed to the influence of the strain induced by epitaxial growth of BST film on LSMO bottom layer.[21] Moreover, the value of δ is calculated as 151 from the fitting curve, which is close to that of the $Au/Ba_{0.5}Sr_{0.5}TiO_3/La_{0.5}Sr_{0.5}CoO_3$ heterostructure.[22] The inset of Fig. 4 shows the Curie-Weiss plots [$\varepsilon_{(T)}^{-1}$ against T] deduced from $\varepsilon_{(E=0)}$ vs T. By fitting the experimental data, the Curie-Weiss constant is estimated as 2.23×10^5 K, which agrees well with other values of BST films of the displacive type.[23] For comparison, the Curie-Weiss constant of the order-disorder type ferroelectric has small values in the range of 10^2-10^3 K.[24]

For practical application, the dielectric tunability should be as large as desired. The dielectric tunability is defined as

$$\text{tunability}=\frac{|\varepsilon_{r(T,0)}-\varepsilon_{r(T,E)}|}{\varepsilon_{r(T,0)}}, \tag{4}$$

where $\varepsilon_{r(T,0)}$ and $\varepsilon_{r(T,E)}$ were defined before. Deduced from the data shown in Fig. 3, the temperature dependence of dielectric tunability (at 200 kV/cm) are calculated and presented in Fig. 5. As shown in the figure, the highest dielectric tunability is about 39.5% near 200 K, while the dielectric constant decreased to 60.4% of the maximum value at dc electric field of 200 kV/cm. Moreover, it is interesting that the dielectric tunability follows the same temperature dependence as that of dielectric constant at zero electric field $\varepsilon_{(E=0)}$ vs T. This phenomenon can also be interpreted by the Johnson phenomenological theory: Combined with relations (2) and (4), the dielectric tunability can be written as

$$\text{tunability}=1-\frac{1}{[1+(\varepsilon_0\varepsilon_{r(T,0)})^3\alpha_{(T)}E^2]^{1/3}}. \tag{5}$$

Equation (5) predicts that the higher the dielectric constant at zero electric field, the larger the dielectric tunability would be. As a result, the temperature dependence of dielectric tunability tunability$_{(E=200\text{ kV/cm})}$ vs T would be similar to that of dielectric constant at zero field $\varepsilon_{(E=0)}$ vs T. We calculated the dielectric tunability as a function of temperature by Eq. (5). As shown in Fig. 5, the calculated dielectric tunability decreases with increasing temperature above T_C and decreasing temperature below T_C, which agrees with our analysis. The inset of Fig. 5 shows the temperature dependence of $\alpha_{(T)}$ defined in Eq. (2). However, from 20 to 200 K, the value of $\alpha_{(T)}$ of BST/LSMO heterostructure decreases monotonously with increasing temperature. This can be understood as follows: in the ferroelectric state below T_C, the polarization of the BST/LSMO heterostructure increases with temperature decreasing. As a result, the enharmonic contributions of the polarization to the free energy $\alpha_{(T)}$ would increase with temperature decreasing. However, above 200 K, the temperature

Downloaded 01 Apr 2011 to 158.132.161.9. Redistribution subject to AIP license or copyright; see http://jap.aip.org/about/rights_and_permissions

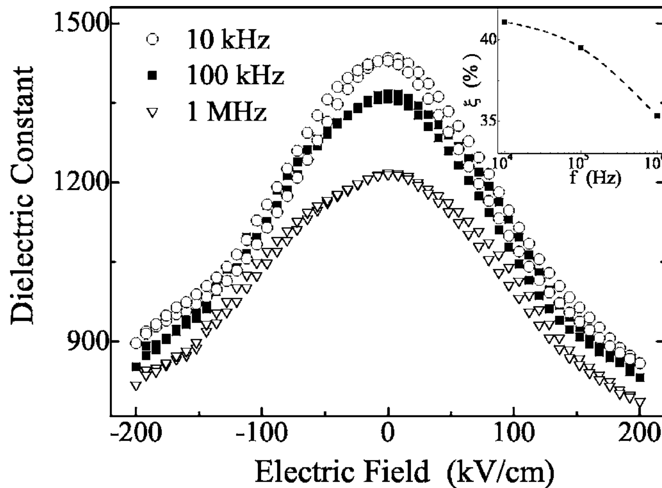

FIG. 6. dc electric field dependence of dielectric constant of BST/LSMO heterostructure at 200 K under 10 kHz, 100 kHz, and 1 MHz. The inset shows the calculated tunability of heterostructure as a function of frequency up to 1 MHz.

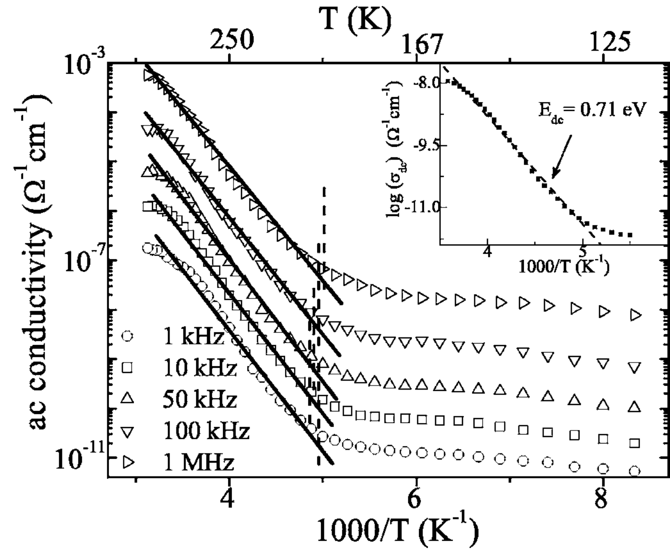

FIG. 7. Temperature dependence of ac conductivity of Pt/BST/LSMO capacitors from 80 to 300 K. In the temperature region where semiconductor-type conduction became dominant, the thermal activation energy of the ac conductivity was about 0.7 eV from 1 kHz to 1 MHz. The inset shows the activated energy of dc conductivity of BST/LSMO heterostructure was about 0.71 eV.

dependent of $\alpha_{(T)}$ became relatively weak, indicating the paraelectric state of the heterostructure. This result was consistent with the report on $SrTiO_3/YBa_2Cu_3O_{7-\sigma}$ bilayers.[25] Figure 6 shows the dielectric permittivity of films as a function of electric field at various frequencies, which are measured at 200 K and dc field of 200 kV/cm. It is clear that the dielectric permittivity of BST/LSMO heterostructure decreases monotonously with increasing the frequency. Moreover, from the inset of Fig. 6, the tunability ξ of BST/LSMO heterostructure decreases from 41.3% at 10 kHz, 39.5% at 100 kHz, to 35.3% at 1 MHz. Therefore, for BST/LSMO heterostructure, the frequency decay of dielectric tunability should be taken into account for the tunable device application in high-frequency region.

Figure 7 shows the temperature dependence of ac conductivity of the BST/LSMO heterostructure at the frequency from 1 kHz to 1 MHz, while the ac conductivity (δ_{ac}) is plotted as a function of $1000/T$. It is apparent that in the lower temperature regime (80–180 K), the ac conductivity of BST film is almost independent of the temperature (but dependent of the frequency), as usually observed in many oxide films.[26] However, with increasing the temperature, an obvious dielectric relaxation of BST/LSMO heterostructure takes place. In the higher temperature regime (200–300 K), the ac conductivity is mainly determined by the temperature, while a semiconductor behavior became apparent. It is well known that the conductivity behavior can be described by a thermally activated process with the relation,

$$\delta = \delta_0 \exp[-E_{cond}/k_B T], \tag{6}$$

where δ_0 is a constant, k_B is the Boltzmann's constant, and E_{cond} is the activated energy for electric conduction. In the higher temperature region, the ac conductivity behavior was fitted with Eq. (6) as indicated by the solid line. As shown in Fig. 7, the slope of the straight line was represented as the activated energy. As a consequence, the values of activated energy E_{cond} of BST/LSMO heterostructure are estimated to be 0.67 and 0.73 eV at 1 kHz and 1 MHz, respectively. Compared with previous literature, the values of activated energy obtained here are larger than that in the crystalline $BaTiO_3$ film (0.23 eV)[27] and are smaller than that of amorphous $SrTiO_3$ film (0.84 eV).[28]

As for the origin of conductivity process, the oxygen vacancies play an important role in BST film, which act as donors with the following relations:

$$O_O = V_O^{\bullet\bullet} + 2e' + \frac{1}{2}O_2, \tag{7}$$

$$Ti^{4+} + e' = Ti^{3+}, \tag{8}$$

where the O_O is oxygen ions at oxygen site, $V_O^{\bullet\bullet}$ is ionized oxygen vacancies, and e' is an electron. Waser *et al.*[29] pointed out that, with increasing temperature, the oxygen vacancies $V_O^{\bullet\bullet}$ would come to influence the electrical conductions through transport onto the conduction edge by the aid of thermal excitation. Therefore, it is reasonable that electrical conduction in BST/LSMO heterostructure is correlated with the thermal activated motions of ionized oxygen vacancies $V_O^{\bullet\bullet}$, which is associated with Ti^{3+} ion so as to form the dipole $V_O^{\bullet\bullet}-2Ti^{3+}$ under an alternating electric field. Similar conduction mechanism has been reported for $BaTiO_3$ (Ref. 27) and $SrTiO_3$ (Ref. 28) films. Moreover, the temperature dependence of dc conductivity of BST/LSMO heterostructure is plotted in the inset of Fig. 7. It can be seen that the slope of the straight line fitted to δ_{dc} (0.71 eV) is very close to that of δ_{ac}. These results indicate that, in the temperature regime where a semiconductor-type conduction becomes prominent, both ac and dc conductivity of BST/LSMO heterostructure have the same conductive mechanism. However, in the lower temperature regime (80–180 K), the mechanism on the temperature independence of the conductivity is still unclear, which should be under investigation further.

Downloaded 01 Apr 2011 to 158.132.161.9. Redistribution subject to AIP license or copyright; see http://jap.aip.org/about/rights_and_permissions

IV. CONCLUSIONS

Both BST and LSMO layers grew epitaxially on the (001) $SrTiO_3$ crystal by pulsed laser deposition method. There existed an interdiffusive layer between BST and LSMO layer on the order of 3 nm, which may be formed during the fabrication of heterostructure. The ε vs E characteristic of BST/LSMO heterostructure exhibited an increasing nonlinear behavior with decreasing temperature from 300 to 20 K. Moreover, a dielectric relaxor behavior was found in $\varepsilon_{(E=0)}$ vs T characterizes with the diffuseness coefficient of 1.73, which may be attributed to the influence of the strain between BST and LSMO layers. The similarity between $\varepsilon_{(E=0)}$ vs T and tunability$_{(E=200\ \mathrm{kV/cm})}$ vs T was discussed using the Johnson theory. Furthermore, in the temperature range where a semiconductor-type conduction became dominant, the thermal activated energy was obtained as 0.67 and 0.73 eV at 1 kHz and 1 MHz, respectively. The origin of the conductivity behavior may be ascribed to the thermally active motions of the dipole $V_O^{\bullet\bullet}-2Ti^{3+}$ under an alternative field.

[1] Y. Gim, T. Hudson, Y. Fan, C. Kwon, A. T. Findikoglu, B. J. Gibbons, B. H. Park, and Q. X. Jia, Appl. Phys. Lett. **77**, 1200 (2000).
[2] M. Izuha, K. Abe, M. Koike, and N. Fukushima, Appl. Phys. Lett. **70**, 1405 (1997).
[3] B. Nagaraj, T. Sawhney, S. Perusse, S. Aggarwal, R. Ramesh, V. S. Kaushik, S. Zafar, R. E. Jones, J. H. Lee, V. B. Alu, and J. Lee, Appl. Phys. Lett. **74**, 3194 (1999).
[4] B. S. Kim, S. H. Oh, S. Y. Son, K. W. Park, Z. R. Dai, and F. S. Ohuchi, J. Appl. Phys. **87**, 4425 (2000).
[5] S. G. Yoon, J. C. Lee, and A. Safari, J. Appl. Phys. **76**, 2999 (1994).
[6] C. S. Hwang, B. T. Lee, and C. S. Kang, J. Appl. Phys. **83**, 3703 (1998).
[7] K. K. Park and J. H. Cho, Appl. Phys. Lett. **77**, 435 (2000).
[8] W. B. Wu, K. U. Wong, X. G. Li, C. L. Choy, and Y. H. Zhang, J. Appl. Phys. **87**, 3006 (2000).
[9] M. A. Zurbuchen, T. Wu, S. Saha, J. Mitchell, and S. K. Streiffer, Appl. Phys. Lett. **87**, 232908 (2005).
[10] A. M. Grishin, S. I. Khartsev, and P. Johnsson, Appl. Phys. Lett. **74**, 1015 (1999).
[11] C. L. Chen, J. Shen, S. Y. Chen, G. P. Luo, C. W. Chu, F. A. Miranda, F. W. Van Keuls, J. C. Jiang, E. I. Meletis, and H. Y. Chang, Appl. Phys. Lett. **78**, 652 (2001).
[12] L. J. Sinnamon, M. M. Saad, R. M. Bowman, and J. M. Gregg, Appl. Phys. Lett. **81**, 703 (2002).
[13] M. W. Cole, P. C. Joshi, M. Ervin, M. Wood, and R. L. Pfeffer, J. Appl. Phys. **92**, 3967 (2002).
[14] J. Miao, W. Chen, L. Zhao, B. Chen, H. Yang, W. Peng, X. Zhu, B. Xu, L. X. Cao, X. G. Qiu, and B. R. Zhao, J. Appl. Phys. **96**, 6578 (2004).
[15] C. M. Chu and P. Lin, Appl. Phys. Lett. **70**, 249 (1997).
[16] M. Es-Souni, E. Girdauskaite, S. Iakovlev, C.-H. Solterbeck, and V. Zaporojtchenko, J. Appl. Phys. **96**, 5691 (2004).
[17] S. L. Miller, R. D. Nasby, J. R. Schwank, M. S. Rodgers, and P. V. Dressendorfer, J. Appl. Phys. **68**, 6463 (1990).
[18] K. M. Johnson, J. Appl. Phys. **33**, 2826 (1962).
[19] A. F. Devonshire, Philos. Mag. **40**, 1040 (1949).
[20] C. B. Parker, J. P. Maria, and A. I. Kingon, Appl. Phys. Lett. **81**, 340 (2002).
[21] J. Miao, H. Yang, W. R. Chen, J. Yuan, L. Zhao, W. Peng, X. H. Zhu, and B. R. Zhao, J. Phys. D **38**, 5 (2005).
[22] A. Lookman, R. M. Bowman, J. M. Gregg, J. Kut, S. Rios, M. Dawber, A. Ruediger, and J. F. Scott, J. Appl. Phys. **96**, 555 (2004).
[23] M. Tyunina and J. Levoska, Phys. Rev. B **70**, 132105 (2004).
[24] K. Jona and G. Shirane, *Ferroelectric Crystals* (Pergamon, Oxford, 1962).
[25] D. Fuchs, C. W. Schneider, R. Schneider, and H. Rietschel, J. Appl. Phys. **85**, 7362 (1999).
[26] J. C. Dyre, J. Appl. Phys. **64**, 2456 (1988).
[27] S. J. Lee, K. Y. Kang, and S. K. Han, Appl. Phys. Lett. **75**, 1784 (1999).
[28] K. Morii, H. Kawano, I. Fijii, T. Matsui, and Y. Nakayama, J. Appl. Phys. **78**, 1914 (1995).
[29] R. Waser, T. Baiatu, and K. H. Hardtl, J. Am. Ceram. Soc. **73**, 1645 (1990).

Downloaded 01 Apr 2011 to 158.132.161.9. Redistribution subject to AIP license or copyright; see http://jap.aip.org/about/rights_and_permissions